Folded acoustic and quantized optic phonons in (GaAl)As superlattices

C. Colvard,* T. A. Gant, and M. V. Klein†
Department of Physics and Materials Research Laboratory, University of Illinois at Urbana—Champaign
1110 West Green Street, Urbana, Illinois 61801

R. Merlin††
Materials Research Laboratory and Coordinated Science Laboratory,
University of Illinois at Urbana—Champaign, Urbana, Illinois 61801

R. Fischer and H. Morkoc
Department of Electrical Engineering and Coordinated Science Laboratory,
University of Illinois at Urbana—Champaign, Urbana, Illinois 61801

A. C. Gossard
AT&T Bell Laboratories, Murray Hill, New Jersey 07974
(Received 5 July 1984)

Raman scattering studies of a variety of (GaAl)As superlattices grown by molecular-beam epitaxy are presented. Folded acoustic phonons appear as doublets in the Raman spectra. Their frequencies are accurately predicted by several models, including an approximate solution of an elastic continuum model through a perturbation approach. Scattering intensities of the folded acoustic modes are predicted by a photoelastic continuum model. Calculations on a layered dielectric continuum provide information about anisotropy of optical phonons. Linear-chain model calculations indicate that optical phonons in binary superlattices are largely confined to alternate layers. Peaks in the Raman data are identified with the resulting quantized optic modes. It is shown that Raman scattering has the potential to provide structural information similar to that which can be obtained by x-ray diffraction.

I. INTRODUCTION

Semiconductor superlattices (SL's) have been of interest for nearly 15 years now, an interest stimulated by the development of techniques, such as molecular-beam epitaxy (MBE) and metalorganic chemical-vapor deposition (MOCVD), capable of growing crystals of alternating layers of two semiconductors with nanometer spatial periods. Potential device applications have spurred studies of the electronic properties of doped and undoped SL's and quantum-well heterostructures. Much less attention has been paid to the vibrational properties, either theoretical or experimental. Calculations have been made for transverse-phonon—polariton branches in GaAs-AlAs SL's,[1] and discrete[2] and continuum[3] models have been used to describe phonon folding and to estimate surface-mode behavior.[4] The creation of a gap in the acoustic-phonon dispersion by the SL was first confirmed by acoustic transmission experiments.[5] Raman scattering, a natural probe for SL phonon studies, has been the most frequently employed experimental tool.

Manuel *et al.*[6] studied the resonant Raman behavior of LO phonons near the energy gap of four GaAs-$Al_xGa_{1-x}As$ samples with $63 < d < 200$ Å and $x \sim 0.25$. They also derived a two-dimensional result for the resonance behavior. An extensive study was made by Barker *et al.*[2] of Raman scattering and infrared absorption in a series of very-thin-layer GaAs-AlAs samples. They calculated the effects of phonon folding and made comparisons between alloy samples and a number of thin-layer SL's. Sai-Halasz *et al.*[7,8] noticed new peaks appearing between the LO^{GaAs} and LO_1^{AlGaAs} modes in resonant Raman spectra of GaAs-$Al_{0.25}Ga_{0.75}As$ samples which they attributed to umklapp processes. These new peaks were shown to be similar to E(LO) phonons by Merlin *et al.*[9] The first clear phonon folding in light scattering experiments was seen by Colvard *et al.*[3] Later Raman studies report scattering from both acoustic[10,11] and optic[10] phonons, including resonant enhancements at quantized exciton levels.[12] Brillouin scattering experiments have been performed by Sapriel *et al.*[11] Indications of optical-phonon folding have been reported by Jusserand *et al.*[13]

We present here a comparison of experimental Raman scattering results from a variety of SL's with several theoretical models, including a perturbation calculation which reproduces the essentials of the acoustic-phonon spectrum, such as sound velocity and gap widths. We show that Raman data can provide information on the layering parameters heretofore gathered primarily from x-ray diffraction. A model based on bulk photoelastic behavior is shown to predict the intensity of the observed folded-acoustic-phonon peaks. The optical phonons are seen to be best described by quantization, as in the electron case, rather than by zone folding.

In the next section several models of SL phonon behavior are outlined. Section III presents a calculation of light scattering intensities, relating the folded-phonon and Brillouin scattering intensity to the bulk photoelastic

constants. Sections IV and V present the experimental results and discussion.

II. PHONON MODELS

Several different approaches to modeling superlattice phonons have been found to be useful, each having certain advantages. A linear-chain model embodies the discrete nature of the crystal structure and provides information about evanescent behavior of optical phonons. It is most useful in frequency regions in which the bulk-phonon dispersion is nonlinear. At low frequencies and long wavelengths the lattice can be treated as an elastic continuum, in which case a Kronig-Penney type of approach yields a convenient analytic expression for phonon folding. The layer thicknesses in this case are not restricted to integral multiples of the monolayer spacing. Alternatively, at these same frequencies, the superlattice can be considered as a perturbation on an average elastic background. This approximation approach yields explicitly the gap widths and sound velocity for an arbitrary composition profile.

These models will be outlined below, in addition to a dielectric continuum model which allows an estimate of the effects of long-wavelength electric fields. Of course, one wants a comprehensive theory of superlattice effects which correctly deals with all microscopic short- and long-range forces. Such a theory is especially needed in dealing with the spectrum of optical phonons. Calculations using such a theory have recently been made by Yip and Chang.[14]

A. Linear-chain model

This model has been applied to binary-binary superlattices by Barker *et al.*[2] It is valid in bulk crystals for phonons propagating along [001], where planes of atoms move as a whole, and the longitudinal and transverse vibrations are decoupled. For longitudinal modes a single nearest-neighbor spring constant provides the only free parameter, whereas two different nearest-neighbor spring constants provide the anisotropy necessary to describe transverse vibrations.[2] These force constants are allowed to be different in GaAs and AlAs layers, and are fit to bulk values of either the LO(Γ) phonon frequency [or TO(Γ) and TA(X) for transverse modes] or the sound velocity v_{long} [or v_{trans} and TO(Γ) frequency]. To fit both optic and acoustic regions, more-distant-neighbor interactions must be included.[15] The relationship between longitudinal and transverse force constants has been neglected here; they have been separately determined in order to force a closer empirical fit of this simplistic model to the zone-edge phonons. The inclusion of such considerations (e.g., requiring $2K^L=K_1^T+K_2^T$) does not affect the conclusions drawn from this model.

By utilizing bulk-phonon solutions (propagating or evanescent) within the layers and matching these at the interfaces, arbitrary layer thicknesses can be considered by solving only a 4×4 determinant. The longitudinal case will be described here; the extension to anisotropic force constants for the transverse case is straightforward. Figure 1 shows the model used. Within each layer

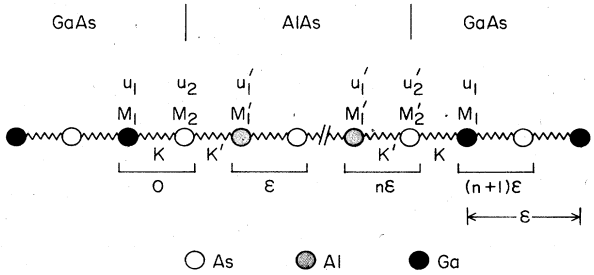

FIG. 1. Model used for linear-chain calculations. AlAs layer thickness is $d_2=n\epsilon$.

$$M_1\ddot{U}_1(m\epsilon)=-K\{2U_1(m\epsilon)-U_2(m\epsilon)-U_2[(m-1)\epsilon]\}\ , \tag{1}$$

$$M_2\ddot{U}_2(m\epsilon)=-K\{2U_2(m\epsilon)-U_1[(m+1)\epsilon]-U_1[m\epsilon]\}\ , \tag{2}$$

where $U(m\epsilon)$ is the displacement along $\hat{z}$ of the atom at $z=m\epsilon$, and ϵ is the monolayer spacing $\epsilon=a/2$. Taking $\pm\alpha$ as the phonon wave vector q_z in GaAs, this yields

$$\cos(\alpha\epsilon)=\frac{(M_1\omega^2-2K)(M_2\omega^2-2K)-2K^2}{2K^2}\ . \tag{3}$$

Defining $\gamma_\pm\equiv U_2/U_1$ for $\pm\alpha$, we find

$$\gamma_\pm=\frac{-K(1+e^{\pm i\alpha\epsilon})}{M_2\omega^2-2K}\ . \tag{4}$$

The above equations are for GaAs; similar expressions describe AlAs with wave vector $q_z=\pm\beta$ and $\delta_\pm\equiv U_2'/U_1'$. Equation (3) is plotted in Fig. 2, which

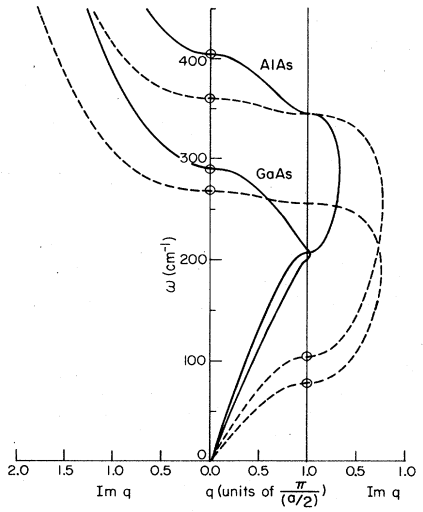

FIG. 2. Real and imaginary part of phonon wave vector q. Dashed lines: transverse modes. Solid lines: longitudinal modes. Parameters of model are fit to circled points. The values used for the force constants were (in 10^5 dyn/cm) as follows: for GaAs, $K^L=0.907$, $K_1^T=0.132$, $K_2^T=1.40$; for AlAs, $K^{L'}=0.954$, $K_1^{T'}=0.171$, $K_2^{T'}=1.35$.

shows both the real and the imaginary part of q_z. The imaginary part indicates the rate of attenuation of a vibration at a particular frequency. For $a/2=2.83$ Å, a penetration depth of one monolayer for the amplitude $U(z)$ corresponds to $\mathrm{Im}q_z=0.32\pi/(a/2)$. The plot indicates that at GaAs optical-mode frequencies the vibrations extend less than one monolayer into the AlAs, where they are damped optical modes with $\mathrm{Re}q=2\pi/a$. At AlAs optical-mode frequencies they are even more localized in the AlAs layer, decaying into the GaAs as damped acoustical modes with $\mathrm{Re}q=0$. The result of this confinement of the optical vibrations is apparent in Fig. 3, where the folded superlattice optical modes are seen to be quite flat.

In a superlattice the displacements become $U_1(z)=Ae^{i\alpha z}+Be^{-i\alpha z}$ and $U_1'(z)=Ce^{i\beta z}+De^{-i\beta z}$. At an interface the forces must be matched, so that each wave behaves as if it were in an infinite medium. Thus at $z=0$:

$$K[U_2(0)-U_1(0)]=K'[U_2'(0)-U_1'(0)] \tag{5}$$

and

$$K[U_1(\epsilon)-U_2(0)]=K'[U_1'(\epsilon)-U_2'(0)] . \tag{6}$$

With the help of Eq. (1) this gives

$$U_2(0)=U_2'(0) \tag{7}$$

and

$$K[U_1(\epsilon)-U_1(0)]=K'[U_1'(\epsilon)-U_1'(0)] \tag{8}$$

which are the discrete analogs of the requirements that displacement and stress be continuous at an acoustical boundary. Similarly, at $z=n\epsilon$ we have

$$U_2(n\epsilon)=U_2'(n\epsilon) \tag{9}$$

and

$$K[U_1(n\epsilon+\epsilon)-U_1(n\epsilon)]=K'[U_1'(n\epsilon+\epsilon)-U_1'(n\epsilon)] . \tag{10}$$

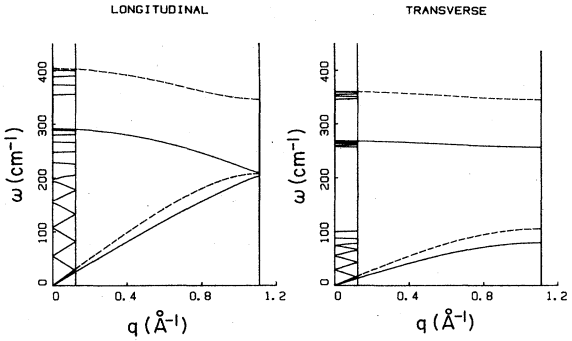

FIG. 3. Linear-chain model calculation of phonon dispersion curves for longitudinal and transverse modes. Large zone: bulk GaAs (solid lines) and AlAs (dashed lines). Small zone: (5,4) superlattice. q given in Å^{-1}.

Imposing the periodic requirement that $U_{\mathrm{SL}}(z+d)=U_{\mathrm{SL}}(z)e^{iqd}$, where q is the superlattice wave vector, and setting layer thicknesses $d_1+d_2=d$, gives the set of equations

$$\gamma_+A+\gamma_-B=\delta_+C+\delta_-D , \tag{11a}$$

$$G_+A+G_-B=H_+C+H_-D , \tag{11b}$$

$$\gamma_+Ae^{-i\alpha d_1}e^{iqd}+\gamma_-Be^{i\alpha d_1}e^{iqd}=\delta_+Ce^{i\beta d_2}+\delta_-De^{-i\beta d_2} , \tag{11c}$$

$$G_+Ae^{-i\alpha d_1}e^{iqd}+G_-Be^{i\alpha d_1}e^{iqd}=H_+Ce^{i\beta d_2}+H_-De^{-i\beta d_2} , \tag{11d}$$

where

$$G_\pm\equiv K(e^{\pm i\alpha\epsilon}-1) \tag{12a}$$

and

$$H_\pm\equiv K'(e^{\pm i\beta\epsilon}-1) . \tag{12b}$$

The solution of these equations is given by

$$\cos(qd)=\cos(\alpha d_1)\cos(\beta d_2)+\frac{2(\gamma_+\gamma_-H_+H_-+\delta_+\delta_-G_+G_-)}{(\gamma_-\delta_-G_+H_++\gamma_+\delta_+G_-H_--\gamma_-\delta_+G_+H_--\gamma_+\delta_-G_-H_+)}\sin(\alpha d_1)\sin(\beta d_2) . \tag{13}$$

In the transverse case, an additional term appears in the sine multiplicand. This solution is shown in Fig. 3 for a (5,4) superlattice. (The notation here means 5 monolayers of GaAs and 4 monolayers of AlAs.) The phonon branches above the first but below about 200 cm^{-1}, although strictly optical branches of the SL, are commonly referred to as folded acoustic branches.

B. Elastic continuum models

The phonon dispersion is approximately linear below about 100 cm^{-1} for LA phonons and below 50 cm^{-1} for TA phonons, and in this region the crystal can be treated as an elastic continuum. Vibrations in layered elastic media have been considered by Rytov,[16] and his results have been shown to apply to acoustic phonons in superlattices.[3] The dispersion is given by

$$\cos(qd)=\cos\left[\frac{\omega d_1}{v_1}\right]\cos\left[\frac{\omega d_2}{v_2}\right]-\frac{1+\kappa^2}{2\kappa}\sin\left[\frac{\omega d_1}{v_1}\right]\sin\left[\frac{\omega d_2}{v_2}\right] \tag{14}$$

which is a solution of the wave equation

$$\rho\ddot{U}=\frac{\partial}{\partial z}\left[K\frac{\partial U}{\partial z}\right] . \tag{15}$$

Here the sound velocity is $v=(K/\rho)^{1/2}$ in each layer, and $\kappa\equiv\rho_2 v_2/\rho_1 v_1$. In the limit of large wavelengths, the superlattice sound velocity $v_{SL}=\omega/q$ becomes

$$v_{SL}=d\left[\frac{d_1^2}{y_1^2}+\frac{d_2^2}{v_2^2}+\left[\kappa+\frac{1}{\kappa}\right]\frac{d_1 d_2}{v_1 v_2}\right]^{-1/2}. \tag{16}$$

If the elastic constants are equal in the two layers, this reduces to

$$v_{SL}=(\langle v^{-1}\rangle_{\rm rms})^{-1}. \tag{17}$$

The above Rytov solution is valid for a square-wavelike compositional modulation with sharp interfaces. Its results can be recovered, and extended to arbitrary composition profiles, by a perturbation approach. We replace Eq. (15) by

$$\frac{\partial}{\partial z}\left[(K_0+\Delta K)\frac{\partial U}{\partial z}\right]+(\rho_0+\Delta\rho)\omega^2 U=0, \tag{18}$$

where K_0 and ρ_0 are the zeroth Fourier components of the elastic constant and density, and $\Delta K(z)$ and $\Delta\rho(z)$ describe the compositional variation. They depend upon the local Al concentration x. The lowest order equation is then

$$\frac{K_0}{\rho_0}\frac{\partial^2 U}{\partial z^2}+\omega^2 U=0, \tag{19}$$

which gives a virtual-crystal sound velocity $v_0^2\equiv K_0/\rho_0$. This agrees with Eq. (17) for equal elastic constants.

We can make the expansions

$$U(z)=\sum_q U_q e^{iqz}, \tag{20a}$$

$$\Delta K=\sum_S K_S e^{iSz}, \tag{20b}$$

$$\Delta\rho=\sum_S \rho_S e^{iSz}, \tag{20c}$$

where S is a reciprocal-lattice vector, $S=2\pi m/d$, and q ranges over the bulk Brillouin zone. Equation (18) then becomes

$$(v_0^2 q^2-\omega^2)U_q+\sum_S\frac{1}{\rho_0}[q(q-S)K_S-\omega^2\rho_S]U_{q-S}=0. \tag{21}$$

The ω^2 in the perturbation term in Eq. (21) can be approximated by

$$\omega^2\approx v_0^2\,|\,q(q-S)\,|\,. \tag{22}$$

This allows the perturbation to be written as $V_S q(q-S)$, where we define $V_S\equiv(K_S\mp V_0^2\rho_S)/\rho_0$. The minus (plus) sign applies if q $(q-S)$ is positive (negative). We keep only the terms in the sum which correspond to states that are strongly mixed by the perturbation, i.e., for which

$$|\,v_0^2 q^2-v_0^2(q-S)^2\,|\lesssim|\,q(q-S)V_S\,|\,. \tag{23}$$

This is true for the states U_q and U_{q-S}, where $S\approx 2q$. Considering only these two terms, we can simplify Eq. (21) and obtain

$$\omega^2=\frac{v_0^2}{2}[q^2+(q-S)^2]\pm\left[\frac{v_0^4}{4}[q^2-(q-S)^2]^2+|\,V_S\,|^2 q^2(q-S)^2\right]^{1/2}, \tag{24}$$

which for exact degeneracy, $S=2q$, becomes

$$\omega^2=v_0^2 q^2\pm|\,V_S\,|\,q(q-S)\,. \tag{25}$$

If we set $q=m\pi/d$ then

$$\omega^2=(v_0^2\pm|\,V_S\,|)\frac{\pi^2 m^2}{d^2} \tag{26}$$

gives the frequencies on either side of a gap, at the SL zone edge for m odd and zone center for m even. Taking ρ_S for a square wave, and assuming $K_S=0$ (i.e., K equal in the two layers), we find

$$|\,V_S\,|=\left|\frac{v_0^2(\rho_b-\rho_a)}{\rho_0\pi m}\sin\left[\frac{m\pi d_1}{d}\right]\right|, \tag{27}$$

where ρ_a and ρ_b are the densities in the two layers, and where

$$\rho_0=d^{-1}(d_1\rho_a+d_2\rho_b)\,. \tag{28}$$

The expected gaps are found by noting that

$$\omega_+-\omega_-=\frac{|\,V_S\,|}{v_0}\frac{\pi\,|\,m\,|}{d} \tag{29}$$

which gives, again for constant K and sharp boundaries,

$$\omega_+-\omega_-=\left|\frac{v_0(\rho_b-\rho_a)}{\rho_0 d}\sin\left[\frac{m\pi d_1}{d}\right]\right|. \tag{30}$$

C. Dielectric continuum model

For layers thick enough that a local dielectric constant is a well-defined quantity, the optical-phonon behavior can be surmised by treating the SL as a layered dielectric continuum. The dielectric constant can be represented in the binary layers by

$$\epsilon(\omega)=\epsilon_\infty\left[1+\frac{\omega_L^2-\omega_T^2}{\omega_T^2-\omega^2-i\omega\Gamma}\right], \tag{31}$$

which for zero damping becomes

$$\epsilon(\omega)=\epsilon_\infty\left[\frac{\omega_L^2-\omega^2}{\omega_T^2-\omega^2}\right]. \tag{32}$$

In the alloy we can use the factorized form[17]

$$\epsilon(\omega)=\epsilon_\infty\frac{(\omega_{L1}^2-\omega^2)(\omega_{L2}^2-\omega^2)}{(\omega_{T1}^2-\omega^2)(\omega_{T2}^2-\omega^2)}, \tag{33}$$

where ω_L and ω_T are the long-wavelength longitudinal and transverse phonon frequencies. The subscripts 1 and 2 refer to the composition-dependent two-mode behavior of the alloy. Maxwell's equations can then be solved for polarization waves propagating parallel or perpendicular to the layers in the $q\to 0$ limit. This has been done in the

absence of phonon dispersion by Rytov.[18]

The results can most conveniently be summarized by noting that, for long waves, the superlattice behaves as a homogeneous, anisotropic crystal. The average dielectric constants are found to be

$$\epsilon_{x,y}=\bar{\epsilon}=d^{-1}(d_1\epsilon_1+d_2\epsilon_2)\ , \tag{34}$$

$$\epsilon_z=(\langle\epsilon^{-1}\rangle_{\rm av})^{-1}=d\epsilon_1\epsilon_2(d_1\epsilon_2+d_2\epsilon_1)^{-1}\ , \tag{35}$$

where $\langle\ \rangle_{\rm av}$ indicates the average, with ϵ_1 and ϵ_2 given by Eqs. (32) or (33).

The zeros and poles of these dielectric constants occur at the longitudinal and transverse frequencies of the composite layered structure, corresponding, respectively, to the vanishing of the average displacement $\bar{D}$ or electric field $\bar{E}$. For polarization in the plane of the layers and $\mathbf{q}$ along the $\hat{\mathbf{z}}$ direction, the poles of Eq. (34) give TO modes of E symmetry at the bulk TO frequencies. For polarization parallel to the superlattice axis, the zeros of Eq. (35) give LO modes of B_2 or A_1 symmetry at the bulk LO frequencies. In both cases the polarization, and electric field where nonzero, exists only in the layer at whose normal frequency the vibration occurs. If phonon dispersion is considered, these modes are the quantized optic phonons due to SL zone folding.

For $\mathbf{q}$ in the layer plane two new modes appear, a B_2(TO)-like mode at the poles of Eq. (35) and an E(LO)-like mode at the zeros of Eq. (34). The solutions are given by

$$\frac{\epsilon_1(\omega)}{\epsilon_2(\omega)}=\begin{cases}-\dfrac{d_1}{d_2}, & B_2(\mathrm{TO}) \qquad (36a)\\[2ex] -\dfrac{d_2}{d_1}, & E(\mathrm{LO}) \qquad (36b)\end{cases}$$

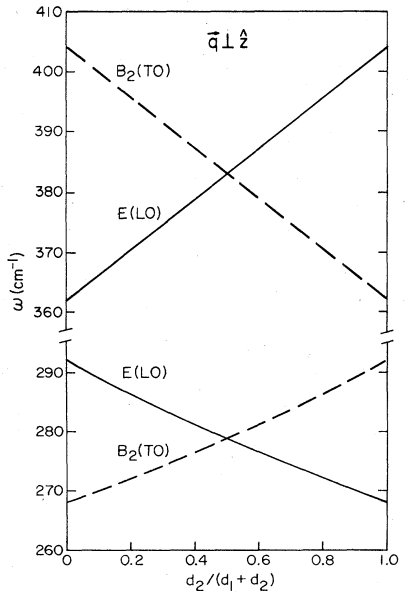

FIG. 4. Frequency of interfacelike optic modes vs AlAs layer thickness: d_1, GaAs layer; d_2, AlAs layer.

with Eqs. (32) or (33) for ϵ_1 and ϵ_2. These frequencies occur between the bulk ω_L and ω_T. For $qd>0$ the polarization decays exponentially away from interfaces, but in the thin-layer limit it is nearly constant throughout the superlattice. Figure 4 plots the frequencies of these modes versus layer thickness for a GaAs-AlAs superlattice. Note that if $d_1\gg d_2$, the LO mode can occur at the TO frequency and vice versa.

Solutions will also exist at the bulk LO and TO frequencies for modes propagating along the layers but spatially quantized along $\hat{\mathbf{z}}$. Ignoring polariton effects, these modes will be similar to the quantized bulk phonons mentioned above at the wave vectors accessible to Raman scattering.

III. PHOTOELASTIC MECHANISM FOR LIGHT SCATTERING

At laser energies far from resonance with superlattice electronic transitions, light scattering from the folded acoustic phonons can be treated as a coherent sum of scattering within bulklike layers due to the photoelastic effect. The photoelastic coefficient is taken to be a function of position z; its value depends on the local Al concentration x:

$$P(z)=P(0)+\frac{dP}{dx}x(z)\ . \tag{37}$$

If the interfaces are abrupt, this will be a square wave:

$$P(z)=\begin{cases}P_a, & 0\le z<d_1\\ P_b, & d_1\le z<d=d_1+d_2\ .\end{cases} \tag{38}$$

The strain due to an LA phonon will cause a proportionate change in the susceptibility:

$$\delta\chi(z)=P(z)\frac{\partial U(z)}{\partial z}\ . \tag{39}$$

Light will be scattered by the qth component of this susceptibility fluctuation that conserves momentum, $\mathbf{q}=\mathbf{k}_i-\mathbf{k}_s$, as in ordinary Brillouin scattering:[19]

$$I(\omega)\propto\langle\,|\,\delta\chi_q\,|^2\rangle_\omega\ . \tag{40}$$

This component is given by

$$\delta\chi_q=\int_{-\infty}^{\infty}e^{-iqz}P(z)\frac{\partial U(z)}{\partial z}dz\ . \tag{41}$$

In the Rytov model, away from gaps in the phonon dispersion curves, this integrand is

$$\delta\chi(z)=\begin{cases}i\alpha P_a e^{i\alpha z}U_{0a}, & 0\le z<d_1\\ i\beta P_b e^{i\beta z}U_{0b}, & d_1\le z<d_2\end{cases} \tag{42}$$

where $\alpha=\omega/v_1$, $\beta=\omega/v_2$, and $v_{1,2}$ are bulk sound velocities. For simplicity the difference between α and β can be ignored, $\alpha\approx\beta\approx q_z$ and $U_{0a}\approx U_{0b}$. $P(z)$ can be separately expanded,

$$P(z)=\sum_m P_m e^{iS_m z},\quad S_m\equiv\frac{2\pi m}{d} \tag{43}$$

allowing the Raman tensor to be written

$$\delta\chi_q = \sum_m P_m i(q - S_m) u_{q-S_m} . \quad (44)$$

The $\pm m$ terms in this sum describe Raman scattering from folded LA phonons at $\omega_m = |q \mp S_m| v_{SL}$ with intensity

$$I_m \propto \omega_m (n_m + 1) |P_m|^2 . \quad (45)$$

(Here n_m is the Bose factor.) The assumption that P is linear in x means that $I_m \sim |x_m|^2$. For $m=0$ this gives the Brillouin scattering cross section in a superlattice at $\omega = qv_{SL}$. For the square-wave case of Eq. (38),

$$P_0 = \frac{1}{d}(d_1 P_a + d_2 P_b) , \quad (46)$$

$$P_m = \frac{i(P_b - P_a)}{2\pi m}[1 - \exp(-i 2\pi m d_1/d)], \quad m \neq 0 \quad (47)$$

giving

$$|P_m|^2 = \left| \frac{(P_b - P_a)}{m\pi} \sin\left[\frac{m\pi d_1}{d} \right] \right|^2, \quad m \neq 0 . \quad (48)$$

For propagation along $\hat{z}$ and backscattering from a (001) face, only LA phonons can be seen, these through the component $P^{xxzz} = P^{12}$ in cubic crystals. Thus the scattered folded-phonon intensity can be compared with that for the Brillouin scattering:

$$I_m / I_{\text{Brill}} = \frac{(P_b^{12} - P_a^{12})^2}{P_0^2} \frac{\sin^2(m\pi d_1/d)}{\pi^2 m^2} \eta . \quad (49)$$

The factor η accounts for the frequency difference between ω_m and ω_{Brill},

$$\eta = [\omega_m (n_m + 1)]/[\omega_0 (n_0 + 1)] .$$

For $\hbar\omega_m \ll kT$, $\eta \approx 1$.

Ren and Harrison have calculated photoelastic constants for GaAs and AlAs.[20] As defined here, their values give $P^{12} = 0.48$ in GaAs and 0.05 in AlAs for the change in χ with strain. For $d_1 = d_2 = d/2$, this gives

$$I_1 / I_{\text{Brill}} \approx 0.3 .$$

IV. EXPERIMENTAL

All samples used in this study were grown by molecular-beam epitaxy on [001]-oriented GaAs substrates. Periods range from 20 to 200 Å, and SL thicknesses vary between 0.5 and 4 μm. Specific SL's will be referred to by their composition. The notation used for an $Al_yGa_{1-y}As$-$Al_xGa_{1-x}As$ SL will be $(d_1{:}y, d_2{:}x)$, where d_1 and d_2 are layer thicknesses. If no value of y is specified, as in most samples, the first number refers to pure GaAs layers ($y=0$).

Light from a cw Ar^+, Kr^+, or dye laser was used to illuminate the samples, which were held in a He cryostat at temperatures between 2–300 K. Scattered light was analyzed by a double-pass $\frac{3}{4}$-m spectrometer equipped with 1800 grooves/mm holographic gratings and was detected by an RCA model No. C31034A photomultiplier tube operated in phonon-counting mode. An Apple II-plus computer was used to collect data and control the experiment. Most measurements were made with light incident at an angle close to Brewster's angle, polarized in the plane of incidence. Scattered light was collected with an $f/1.4$, 85-mm focal length lens whose axis was normal to the surface of the sample. Successive rotations of a polarizer in the scattered beam allowed polarized and depolarized spectra to be interspersed in the same spectral scan, so that small frequency shifts between the two spectra could be detected.

Pieces of one (41 Å, 8 Å:1) sample were annealed at 850 °C for times from 0.25 to 16 h. During the anneals, the samples were placed between two pieces of GaAs in an atmosphere of flowing forming gas inside a quartz furnace. No visible surface degradation or increased surface scattering was seen after annealing for up to 16 h.

V. RESULTS AND DISCUSSION

A. Acoustic region (5–220 cm^{-1})

In this region are seen the most striking features of a superlattice spectrum: the folded acoustic phonons. They appear as doublets in the A_1 spectrum at frequencies from 5 to 100 cm^{-1}. An example is seen in Fig. 5, which exhibits three folded orders, as shown in the inset. The data are taken from a (42 Å, 8 Å:0.3) sample. Observation of small peaks close to the laser line is greatly aided by the quality of the MBE-grown sample surface. Peaks as low as 7 cm^{-1} have been clearly seen. At these small shifts, the intensity of the light scattering is enhanced by the thermal factor $n + 1$, which at room temperature is 21.5 at 10 cm^{-1}, compared to 1.3 at the 292 cm^{-1} GaAs LO-phonon frequency. The data presented here include this factor, which must be kept in mind when interpreting relative intensities.

Figure 6 shows some further examples of the folded doublets, all spectra taken out of resonance at 5145 Å. The widths of the peaks are quite small, usually 2 to 3

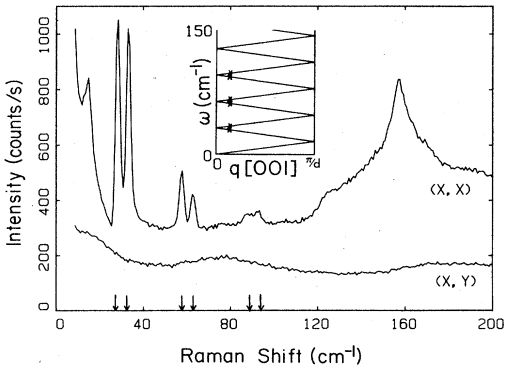

FIG. 5. Raman spectrum of sample (42 Å, 8 Å:0.3); $\lambda_L = 5145$ Å, $T = 300$ K. Inset is Rytov-model calculations showing q of folded LA peaks. The arrows indicate predicted peak frequencies corresponding to a superlattice period of 52.2 Å determined from x-ray diffraction data.

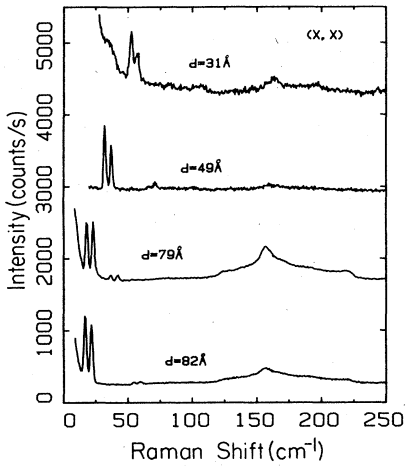

FIG. 6. Samples (20 Å, 12 Å:1), (41 Å, 8 Å:1), (59 Å, 20 Å:0.3), and (41 Å, 41 Å:0.3); $\lambda_L = 5145$ Å, $T = 300$ K. Sharp peaks are folded LA phonons, 2TA is at 160 cm^{-1}.

cm^{-1}, including an instrumental linewidth of about 2 cm^{-1}. The expected contribution to the width due to absorption broadening of q is less than 0.5 cm^{-1}. The acoustic phonons apparently experience a well-defined average period, and show little inhomogeneous broadening. Also seen in the spectra is the well-known 2TA structure, which peaks at 160 cm^{-1} in GaAs and at about 200 cm^{-1} in AlAs. After correcting for the $n+1$ Bose factor, we find that the intensity of the first folded peak varies from 0.01 to 0.13 times the allowed GaAs LO intensity in the samples studied, averaging about 0.05. Under resonant enhancement these two intensities can become comparable.

As pointed out in the preceding section, the folded doublets correspond to scattering from acoustic phonons with wave vectors $2\pi m/d \pm q$. For frequencies away from the gaps, i.e., where the acoustic dispersion is linear, these longitudinal modes are running waves with equal components of A_1 and B_2 character. Light scattering from the Raman-active A_1 component gives equal intensities for the members of each doublet.[11] This can be seen in the lower curves of Fig. 6. The upper curves show the relative intensities of the doublets becoming progressively more unequal in samples with smaller periods. This indicates some admixture of a standing wave due to Bragg reflection and the opening of a gap in the dispersion curve. Figure 7 illustrates the first zone-center gap in a (5,4) superlattice. The solid curve is from a calculation using the linear-chain model, which fits the bulk sound velocity of GaAs with the spring constant being the only adjustable parameter. The data points were taken from a sample with 25.5 Å period by varying the laser wavelength from 4579 to 6764 Å. In such thin-period samples, the wave-vector transfer q is just barely in the region where the dispersion begins to flatten out into the gap. In the case of thicker GaAs layers, i.e., $d_1 > d_2$, the upper curve takes on B_2 symmetry, the lower one A_1 symmetry. Because in acoustic modes the atoms in a unit cell move in phase, the B_2 mode is effectively of odd symmetry under inversion. This gives a vanishing cross section, since purely odd modes cannot ordinarily participate in Raman scattering. One can predict that small period samples having $d_1 < d_2$ will display the opposite asymmetry, the lower frequency peak having mostly B_2 symmetry and thus being weaker.

The wave-vector transfer in backscattering is too large to truly probe the folded gap. In forward scattering, although q_z can be made small, spurious laser light can overwhelm data taken at small frequency shifts. Another possible way to study the gaps is to make samples with large enough period so that $q_z = 4\pi n/\lambda_L \simeq \pi/d$, allowing scattering from the zone-*edge* gap. This would require $d \simeq 250$ Å at $\lambda_L = 4579$ Å in a sample with $n \simeq 4.5$, well within the realm of current technology.

The data presented thus far are all on longitudinal phonons. Some folded transverse phonons have been seen in a Brewster angle scattering geometry. Figure 8 shows an example. The transverse phonons labeled by T appear in both (x,x) and (x,y) spectra. They have E symmetry in the superlattice, and are seen due to the deviation from true backscattering.

A comprehensive confrontation of theory versus experiment for the folded-phonon frequencies is difficult, considering the variety of periods, layer-thickness ratios, and

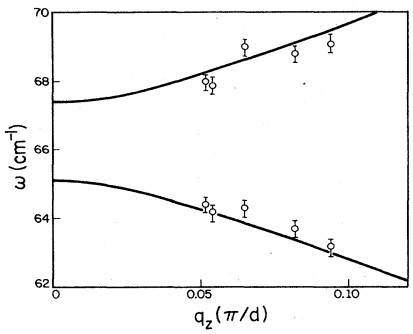

FIG. 7. Phonon dispersion near first folded LA gap for a (5,4) superlattice, calculated with linear-chain model. Data points are folded peaks in sample (14 Å, 12 Å:1) at several laser wavelengths. q_z is in units of π/d.

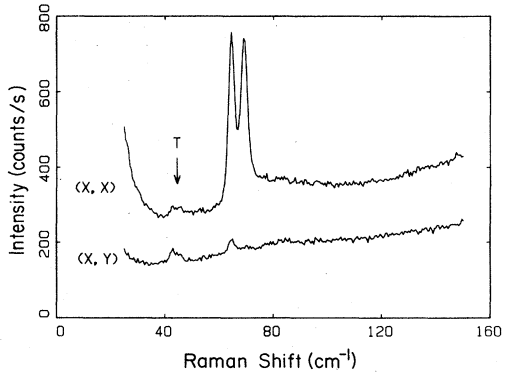

FIG. 8. Raman spectrum of sample (14 Å, 12 Å:1); $\lambda_L = 5145$ Å, $T = 300$ K, near first folded gap. Strong peaks are LA phonons, T indicates transverse phonons.

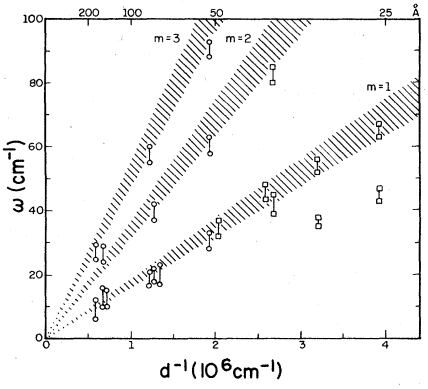

FIG. 9. Composite plot of folded-acoustic-phonon frequencies vs inverse period. Circles refer to samples with alloy barriers, squares to those with pure AlAs barriers. The two doublets at lower right are transverse modes. Shaded regions are bounded by folded AlAs and GaAs bulk sound waves $\omega=(2\pi m/d)v_s$.

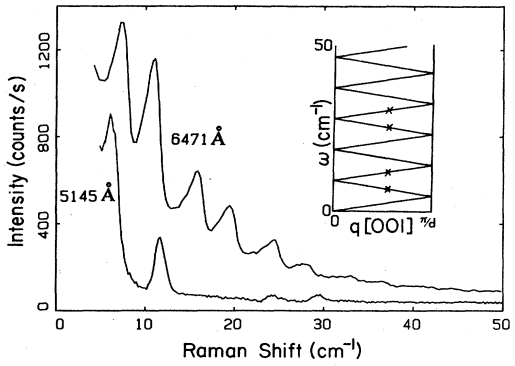

FIG. 11. Raman spectra of sample (85 Å, 88 Å:0.3) for two values of λ_L; (x,x) geometry, $T=300$ K. Inset is Rytov-model calculation showing q of peaks in lower curve and missing modes. Upper resonant spectrum shows interference-type behavior.

alloy compositions studied. In addition, the bulk sound velocity in AlAs is not well known. It is often estimated (as here) by $v_s^2=C/\rho$, using the same elastic constant C as in GaAs. (The values of elastic constants $C_{11}=12.5$, $C_{12}=5.34$, and $C_{44}=5.42\times10^{11}$ dyn/cm^2 are given in Ref. 20 for AlAs, estimated from empirical relations and typical III-V values. This C_{11} is 6% larger than in GaAs.) Figure 9 gives a plot of the folded-phonon frequencies observed versus inverse period. The shaded bands indicate the frequencies expected for the first three foldings of an average linear-acoustic branch. They are bounded by $\omega_\pm=v_\pm(2\pi m/d)$, where v_+ is the sound velocity of AlAs, v_- that of GaAs. The midpoint of each doublet is expected to lie within such a band, its exact position depending on the [Al]-to-[Ga] ratio in the sample. The doublets off to the lower right represent transverse phonons.

The doublet splitting is seen to be ~5 cm^{-1} in all observed cases. This is consistent with the wave-vector transfer $q=4\pi n/\lambda_L$ for backscattering. The phonon doublets are at $\omega=v_{\rm SL}(S_m\pm q)$, giving

$$\Delta\omega=2v_{\rm SL}q=8\pi n v_{\rm SL}/\lambda_L \tag{50a}$$

$$\simeq5\ \text{cm}^{-1}\ . \tag{50b}$$

It is believed that the scatter in the data is largely due to uncertainty in the value of the sample period. When this was not determined by x-ray diffraction, it was estimated from growth conditions. Furthermore, a sample's period can vary across its surface. Figure 9 demonstrates the ability of Raman scattering in a superlattice to provide structural information, similar to that from x-rays, by measuring the sample period. It has the advantage of providing convenient spatial resolution as well.

Another feature of interest in Fig. 9 is the appearance of two samples showing $m=1$ and 3 phonon doublets, but none with $m=2$. Figure 10 presents data from sample (41 Å, 41 Å:0.3). The inset is a dispersion calculation, using the Rytov model, with the observed peaks indicated. Missing peaks are also seen in the data of Fig. 11 on a (85 Å, 88 Å:0.3) sample. The inset corresponds to the lower curve, taken out of resonance at $\lambda_L=5145$ Å. (Note, incidentally, that the data are taken with q over

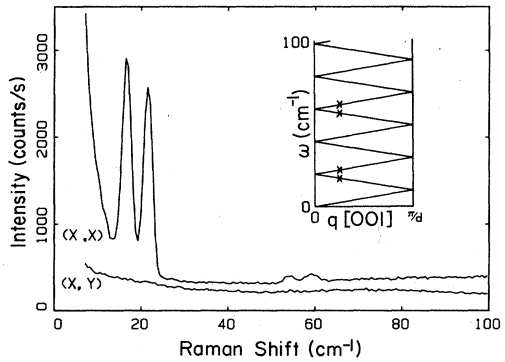

FIG. 10. Raman spectrum of sample (41 Å, 41 Å:0.3); $\lambda_L=5145$ Å, $T=300$ K. Inset is Rytov-model calculation showing q of folded LA phonons and missing second-order peaks.

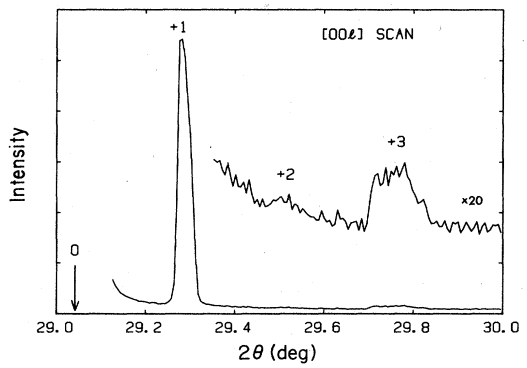

FIG. 12. X-ray diffraction spectrum of sample (85 Å, 88 Å:0.3) showing negligible second-order satellite.

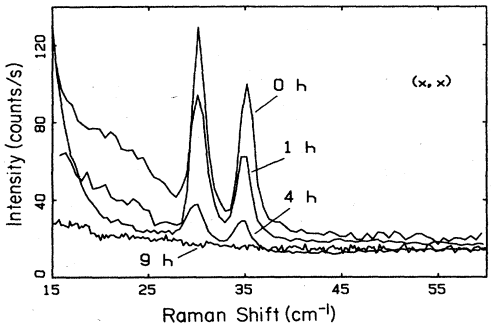

FIG. 13. Raman spectra of folded LA phonons from sample (41 Å, 8 Å:1) annealed at 850 K for 0, 1, 4, and 9 h; $\lambda_L = 5145$ Å, $T = 300$ K; (x,x) geometry.

halfway into the superlattice Brillouin zone.) These data lend support to the model of photoelastic scattering presented in Sec. II. Both samples have nearly equal layer thicknesses; Eq. (48), along with Eq. (45), shows that in this case the scattering vanishes for even values of m. The x-ray diffraction data in Fig. 12 were taken from this sample. Here also the second satellite is missing, corroborating these results. In the samples studied, the ratio of the intensity of the $m=1$ peak to that of the $m=2$ peak is generally consistent with Eq. (45), after corrections are made for the thermal factor in Eq. (45). The intensities of the second and third peaks in Fig. 5 fall off slightly faster than predicted, presumably due to the sensitivity of $\sin^2(\pi m d_1/d)$ to the exact layer thicknesses, especially for larger m.

To see the effect of a nonsharp interface, several pieces of sample (41 Å, 8 Å:1), which contains pure AlAs barrier layers, were annealed at 850 °C for several intervals, up to 16 h. This causes the interfaces to diffuse.[21] The effect on the folded phonons is seen in Fig. 13. The intensity decreases, while the frequency and width (within the experimental limits) do not change. This agrees with predictions of the photoelastic scattering model. The background at frequencies below that of the phonons also decreases. The data were taken at room temperature and are normalized to 50 counts/s at 265 cm^{-1} [the TO(GaAs) peak]. No significant increase was seen in disorder-activated (DA) scattering (DALA and DATA).

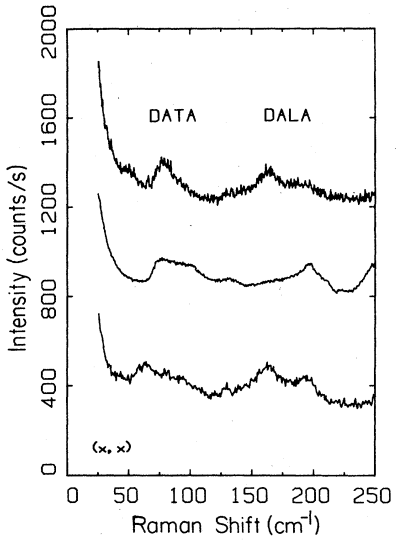

FIG. 15. Raman spectra of three samples showing disorder-activated structure. From top to bottom the samples are (11 Å, 10 Å:1), (38 Å:0.25, 13 Å:1), and (14 Å:0.5, 14 Å:1); $\lambda_L = 5145$ Å, $T = 300$ K.

Under resonant conditions the intensity of the folded-phonon scattering can be significantly altered. An example is the upper curve of Fig. 11, taken near the $E_0 + \Delta_0$ gap of the superlattice. The even-m phonons are now seen, but the peaks are asymmetric, and they are shifted in a way that cannot be explained entirely by a shift in q. Resonance of the laser photon with excitation to a particular SL state, which is an approximate combination of bulk propagating and evanescent states in the two layers, invalidates the assumptions of Sec. III. The asymmetry suggests a coupling between the discrete phonons and a background continuum. Although not pursued here, other examples of such a coupling have been seen, as in Fig. 14. The features near 32 cm^{-1} appear to be antiresonances associated with acoustic phonons at the SL zone *edge*, at half the frequency of the sharp zone center $m=1$

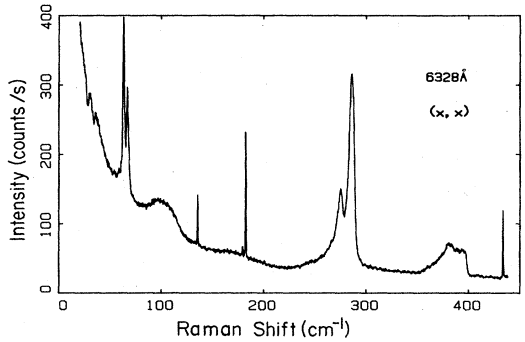

FIG. 14. Raman spectra near the band gap of sample (14 Å, 12 Å:1); $\lambda_L = 6328$ Å, $T = 300$ K. Spikes above 100 cm^{-1} are Ne calibration lines.

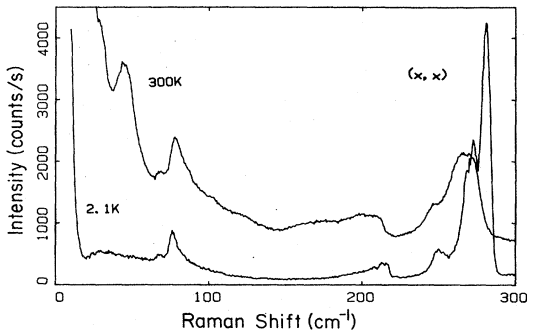

FIG. 16. Raman spectra of sample (12.5 Å, 37.5 Å:1) showing disorder-activated structure at two temperatures; $\lambda_L = 5145$ Å.

peaks. The bump at 100 cm^{-1} is due to second-order optical-phonon difference scattering at ω_{LO}(AlAs)-ω_{LA}(GaAs).

Not all samples studied show the sharp folded phonons and low background that we consider to be indicative of high-quality growth. Figure 15 shows data from three samples whose Raman spectra are dominated by disorder-activated scattering. The lower two curves are from samples (14 Å:0.5, 14 Å:1) and (38 Å:0.25, 13 Å:1), which contain no pure GaAs layers. DALA and DATA structure is also seen in samples with thick AlAs layers, as in Fig. 16. This implies that the disorder which relaxes the momentum conservation does not arise solely within alloy layers, but may be more generally related to the difficulty of growing high-quality layers with high Al content.

B. Optic region (220—420 cm^{-1})

Due to the two-mode behavior of $Al_xGa_{1-x}As$ alloys, the effect of layering on phonons near the GaAs optical frequency in GaAs-$Al_xGa_{1-x}As$ SL's will depend strongly upon the value of x in the barrier layers. For $x<1$ both layers may support GaAs-like optical vibrations, resulting in a dispersive ω versus q with small gaps. In this case, the normal mode may have a different number of nodes in the two layers. For AlAs-like vibrations, and for GaAs-like vibrations in samples with $x\approx 1$, the phonons are highly damped in the nonpropagating layer. As indicated in Fig. 2, these damped modes are opticlike [Re(q)$=\pi/(a/2)$] in AlAs layers and acousticlike (q purely imaginary) in GaAs layers. The localization in alternative layers produces flat optical branches. Whereas Brillouin-zone folding adequately describes the effect of SL layering on the acoustic phonons, the optic branches are better regarded as spatially quantized, analogous to the quantization of electrons in potential wells.

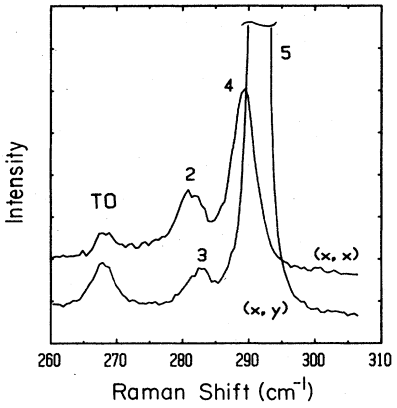

FIG. 18. Raman spectrum near GaAs-like optic branch of sample (20 Å, 12 Å:1). $\lambda_L=6764$ Å, $T=180$ K.

Figure 17 shows data from four GaAs-AlAs samples with GaAs layer thickness increasing from top to bottom. The dominant peaks occur in the (x,y) geometry, indicating they have B_2 symmetry. TO phonons occur in both (x,x) and (x,y) at $\sim$265 and $\sim$357 cm^{-1}. In the upper two curves, weak A_1-symmetry peaks are seen in (x,x). These two samples have been studied under resonant conditions. Figure 18 shows a more detailed spectrum of sample (20 Å, 12 Å:1), taken near the band gap. Two peaks are seen in each geometry, in addition to the TO phonon. The resonant behavior of these phonons is given in Fig. 19. The data were taken with $\lambda_L=6765$ Å by varying the temperature between 100 and 300 K. The temperature dependence of all peak frequencies, -0.015 cm^{-1}/K, agrees with that of GaAs. The luminescence peak at an energy of 1.805 eV at 300 K was used to moni-

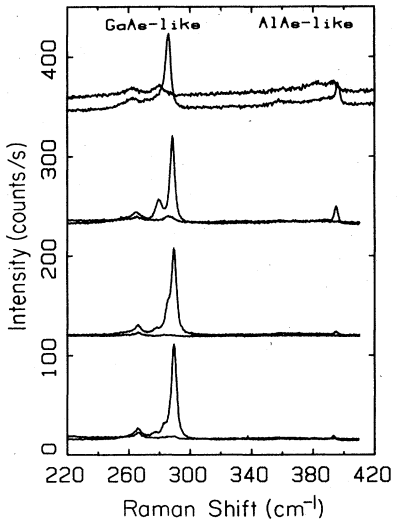

FIG. 17. Optical-phonon Raman spectra of four samples with AlAs barriers. Strong peaks are in (x,y) geometry, weak curve is (x,x). From top to bottom the samples are (14 Å, 12 Å:1); (20 Å, 12 Å:1); (27 Å, 11 Å:1); (41 Å, 8 Å:1).

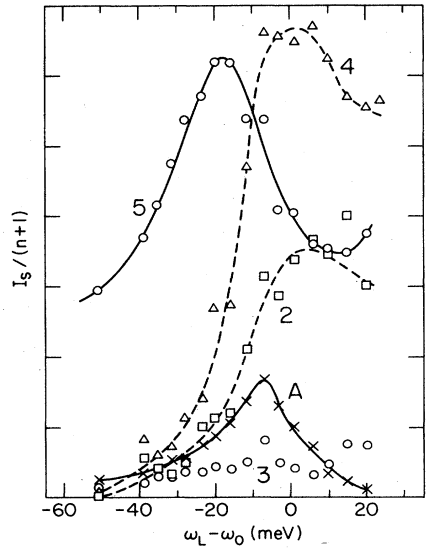

FIG. 19. Resonance behavior of peaks labeled in Fig. 18. A refers to lowest folded acoustic phonon. Band gap was tuned through λ_L by varying temperature. Intensity not corrected for absorption. ω_0 is 300-K luminescence peak.

tor the change in band gap. Both the TO phonon and peak 3 show little resonance enhancement. Peaks 2 and 4 resonate together, reaching a maximum 20 meV above that of peak 5.

Sample (14 Å, 12 Å:1) shows a similar optical-phonon structure and resonance behavior, except that peaks 2 and 4 shift to higher frequencies with lower exciting energies (as the laser is tuned through the band gap), and their resonance maximum is about 50 meV higher than that of peak 5.

A simple prediction of the quantized frequencies is difficult for lack of a numerically accurate model. An upper limit for confinement-induced shifts can be obtained by regarding the bulk LO dispersion as

$$\omega^2=\omega_L^2-v_s^2q^2\ , \tag{51}$$

where v_s is the longitudinal sound velocity. This is the small-q limit of a linear-chain model, but it overestimates the dispersion. The folded frequencies are then given by

$$\omega^2=\omega_L^2-v_s^2\left[\frac{l\pi}{d_1}\right]^2\ , \tag{52}$$

where l is the folding order and d_1 is the single-layer thickness. Using the exact linear chain, we find the result to be somewhat less dispersive, but it is still not accurate enough, giving an uncertainty of several cm^{-1} depending on the fitting parameters. The existing neutron data on GaAs LO-phonon dispersion[22] disagree with Raman results by 6 cm^{-1} at $q=0$; they imply a nearly flat LO branch out to one-third of the bulk zone edge.

Figure 20 is a plot of observed optical-phonon frequencies in the binary layer sample. The straight lines are from Eq. (52), using bulk values of v_s and ω_L, for several values of l. Note that ω^2 is plotted versus inverse squared layer thickness. Peaks not otherwise indicated appear in the B_2-allowed (x,y) geometry. Peaks labeled by E have been previously assigned to E-symmetry phonons, as mentioned below. Points along the lower edge of both regions correspond to TO phonons.

The thickness dependence of the highest B_2 mode frequencies is rather well described by the $l=1$ line. These include the peak labeled 5 in Fig. 18. The dotted arrows suggest that the deviation shown by sample (11 Å, 10 Å:1) from this line may be due to an incorrect determination of its relative layer thicknesses. Keeping d constant but adjusting d_1/d_2 takes the triangles into the crosses. X-ray diffraction provides a precise determination of superlattice period from the satellite spacing. The measurement of individual layer thicknesses can be done by Fourier analysis of satellite intensities or by estimating the average aluminum content from the average lattice constant. The x-ray data are sometimes not good enough to do this accurately. As pointed out in relation to Fig. 14, a good understanding of phonon folding can allow Raman scattering to provide this structural information.

The remaining peaks between the highest frequency B_2 mode and the TO mode are difficult to assign. A rough correlation exists between the $l=2$ line and the second B_2 peak. Consideration of the mode symmetries and the fact that Eq. (52) overestimates the dispersion suggest that the A_1 mode labeled 4 in Fig. 18 should correspond to $l=2$. The second B_2 peaks, labeled 3 in the previous figure, then correspond to $l=3$.

Previous reports[9] have suggested the E-symmetry modes propagating parallel to the interfaces may appear in backscattering spectra due to disorder. Such modes have yet to be systematically verified, although such scattering may contribute to the structure typified by Fig. 18. No additional optical-phonon peaks were seen in any of the alloy-barrier samples included in this study, as were seen in earlier studies. This may be due to the high quality of the present interfaces.

The interfaces in sample (41 Å, 8 Å:1) were intentionally blurred by annealing, and the optical-frequency data are presented in Figs. 21 and 22. The curves were taken in the (x,y) geometry and are normalized to 50 counts/s at 265 cm^{-1} (TO phonon). Pieces of the sample were an-

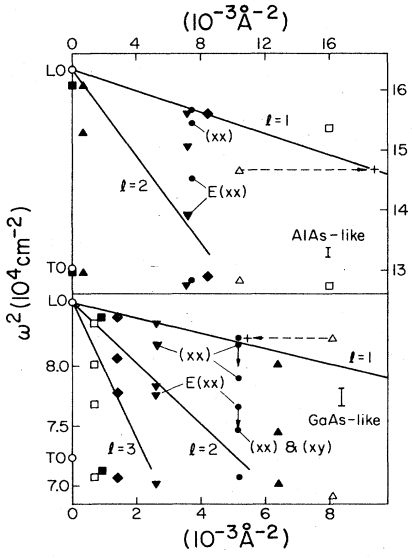

FIG. 20. Composite plot of optical-phonon frequencies squared vs inverse square layer period. d_1 equals GaAs layer thickness, d_2 equals that of AlAs. Straight lines are $\omega^2=\omega_L^2-v_s^2(l\pi/d_{1,2})^2$ for $l=1$, 2, or 3. Unless specified, peaks appear in (x,y) geometry.

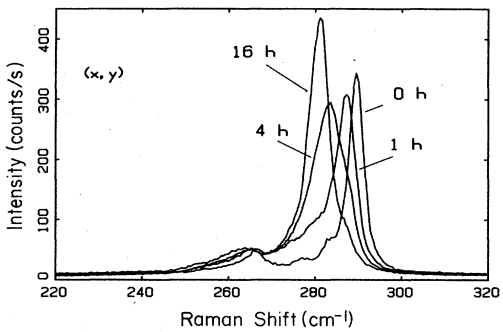

FIG. 21. Raman spectra of GaAs-like optic phonons from sample (41 Å, 8 Å:1) annealed at 850 K for 0, 1, 4, and 16 h; $\lambda_L=5145$ Å, $T=300$ K, (x,y) geometry.

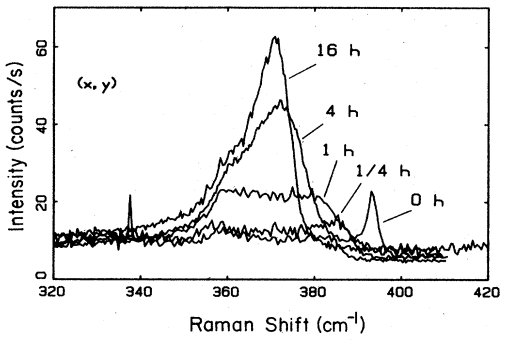

FIG. 22. Same as Fig. 21 for AlAs-like optic region.

nealed for 0.25, 1, 4, 9, and 16 h at 850 °C. The LO phonons are seen to shift toward lower frequency, and a low-frequency tail appears on the TO phonon. The data are approaching the average alloy spectrum with increasing annealing. For an average Al concentration of $x=0.16$, confirmed in this sample by x-ray diffraction,[23] the alloy LO peaks are expected at 285 and 370 cm^{-1}.[17] The LO phonon in Fig. 37 of Ref. 17 has moved below this value to 281 cm^{-1}, perhaps indicating a superlattice effect. Even after 16 h the composition profile should remain sinelike.[24] No trace of the behavior of an $x=0.5$ alloy is seen, which might be expected from equal interpenetration at an interface. This would give peaks at 271 and 388 cm^{-1}.

VI. CONCLUSIONS

In summary, we have examined several models for phonon behavior in semiconductor SL's and compared these with Raman scattering data from a number of aluminum gallium arsenide based SL samples. The models describe well the data in the acoustic-phonon region. The zero-order $\omega(q)$ curve folded into the first minizone forms a good first approximation to the dispersion curves. A photoelastic approach describes the Raman intensities from the resulting folded-phonon doublets. The Raman data are shown to provide structural information similar to that gained from x-ray diffraction. In the optic region, the correspondence between the models and data is not as good. The behavior of the optic-mode frequencies and symmetries seems to be best described in terms of quantized levels, similar to those of confined electrons, due to confinement within one type of layer. This confinement depends on the alloy concentration and phonon frequency, due to two-mode behavior. Better theories, which include the effects of electric fields, are needed to describe the optical behavior.

ACKNOWLEDGMENTS

We thank S. L. Cooper, D. A. Neumann, and H. Zabel for providing x-ray diffraction data. This work was supported by National Science Foundation Grants Nos. DMR 82-03523 and 80-20250, Office of Naval Research Grant No. N00014-80-C-0701, the Joint Services Electronics Program under Grant No. N-00014-79-C-0424, and the Air Force Office of Scientific Research under Grant No. F49620-83-K-201.

*Present address: Siemens Research and Technology Laboratories, 105 College Road East, Princeton, NJ 08540.

†Also at Coordinated Science Laboratory, University of Illinois at Urbana—Champaign.

††Present address: Department of Physics, University of Michigan, Ann Arbor, MI 48109.

[1]R. Tsu and S. S. Jha, Appl. Phys. Lett. **20**, 16 (1972).

[2]A. S. Barker, Jr., J. L. Merz, and A. C. Gossard, Phys. Rev. B **17**, 3181 (1978).

[3]C. Colvard, R. Merlin, M. V. Klein, and A. C. Gossard, Phys. Rev. Lett. **45**, 298 (1980).

[4]J. Sapriel, B. Djafari-Rouhani, and L. Dobrzynski, Surf. Sci. **126**, 197 (1983).

[5]V. Narayanamurti, H. L. Störmer, M. A. Chin, A. C. Gossard, and W. Wiegmann, Phys. Rev. Lett. **43**, 2012 (1979).

[6]P. Manuel, G. A. Sai-Halasz, L. L. Chang, C.-A. Chang, and L. Esaki, Phys. Rev. Lett. **37**, 1701 (1976).

[7]G. A. Sai-Halasz, A. Pinczuk, P. Y. Yu, and L. Esaki, Solid State Commun. **25**, 381 (1978).

[8]G. A. Sai-Halasz, A. Pinczuk, P. Y. Yu, and L. Esaki, Surf. Sci. **73**, 232 (1978).

[9]R. Merlin, C. Colvard, M. V. Klein, H. Morkoc, A. Y. Cho, and A. C. Gossard, Appl. Phys. Lett. **36**, 43 (1980).

[10]C. Colvard, R. Merlin, M. V. Klein, and A. C. Gossard, J. Phys. (Paris) Colloq. **C6**, C6-631 (1981).

[11]J. Sapriel, J. C. Michel, J. C. Toledano, R. Vacher, J. Kervarec, and A. Regreny, Phys. Rev. B **28**, 2007 (1983).

[12]J. E. Zucker, A. Pinczuk, D. S. Chemla, A. Gossard, and W. Wiegmann, Phys. Rev. Lett. **51**, 1293 (1983).

[13]B. Jusserand, D. Paquet, J. Kervarec, and A. Regreny, J. Phys. (Paris) Colloq. **C5**, C5-145 (1984); B. Jusserand, D. Paquet, and A. Regreny, Phys. Rev. B **30**, 6245 (1984).

[14]S. K. Yip and Y. C. Chang, Phys. Rev. B **30**, 7037 (1984).

[15]K. Kunc and R. M. Martin, in *Proceedings of the 16th International Conference on the Physics of Semiconductors,* edited by M. Averous (North-Holland, Amsterdam, 1983), p. 511.

[16]S. M. Rytov, Akust. Zh. **2**, 71 (1956) [Sov. Phys.—Acous. **2**, 67 (1956)].

[17]O. K. Kim and W. G. Spitzer, J. Appl. Phys. **50**, 4362 (1979).

[18]S. M. Rytov, Zh. Eksp. Teor. Fiz. **29**, 605 (1955) [Sov. Phys.—JETP **2**, 466 (1956)].

[19]W. Hayes and R. Loudon, *Scattering of Light by Crystals* (Wiley, New York, 1978).

[20]S.-Y. Ren and W. A. Harrison, Phys. Rev. B **23**, 762 (1981).

[21]*Landolt-Börnstein Tables,* edited by O. Madelung (Springer, Berlin, 1982), Group III, Vol. 17a.

[22]G. Dolling and J. L. T. Waugh, in *Lattice Dynamics,* edited by R. F. Wallis (Pergamon, New York, 1965), p. 19.

[23]W. J. Bartels (private communication).

[24]R. M. Fleming, D. B. McWhan, A. C. Gossard, W. Wiegmann, and R. A. Logan, J. Appl. Phys. **51**, 357 (1980).